



**HAL**  
open science

# Fast and Complete Destruction of the Anti-Cancer Drug Cytarabine from Water by Electrocatalytic Oxidation Using Electro-Fenton Process

Sule Camcioglu, Baran Özyurt, Nihal Oturan, Clément Trelu, Mehmet Oturan

## ► To cite this version:

Sule Camcioglu, Baran Özyurt, Nihal Oturan, Clément Trelu, Mehmet Oturan. Fast and Complete Destruction of the Anti-Cancer Drug Cytarabine from Water by Electrocatalytic Oxidation Using Electro-Fenton Process. *Catalysts*, 2022, 12 (12), pp.1598. 10.3390/catal12121598 . hal-04122757

**HAL Id: hal-04122757**

**<https://univ-eiffel.hal.science/hal-04122757>**

Submitted on 8 Jun 2023

**HAL** is a multi-disciplinary open access archive for the deposit and dissemination of scientific research documents, whether they are published or not. The documents may come from teaching and research institutions in France or abroad, or from public or private research centers.

L'archive ouverte pluridisciplinaire **HAL**, est destinée au dépôt et à la diffusion de documents scientifiques de niveau recherche, publiés ou non, émanant des établissements d'enseignement et de recherche français ou étrangers, des laboratoires publics ou privés.

# **Fast and complete destruction of the anti-cancer drug Cytarabine from water by electrocatalytic oxidation using electro-Fenton process**

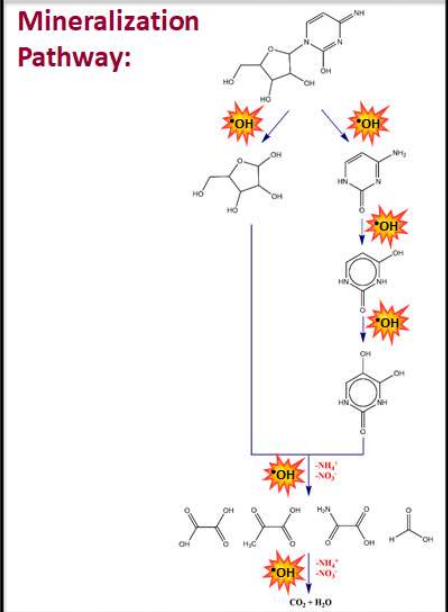
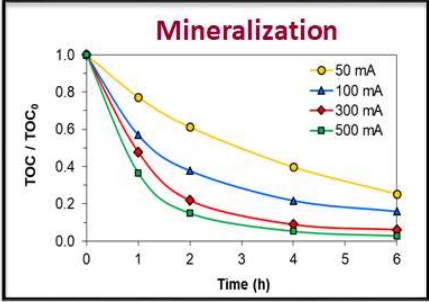
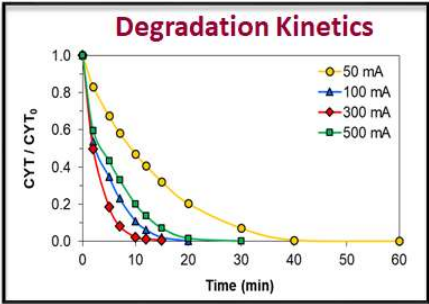
Sule Camcioglu<sup>1,2</sup>, Baran Özyurt<sup>1,2</sup>, Nihal Oturan<sup>1</sup>, Clément Trelu<sup>1</sup>  
Mehmet A. Oturan<sup>1,\*</sup>

<sup>1</sup> Université Gustave Eiffel, Laboratoire Géomatériaux et Environnement EA 4508,  
77454, Marne-la-Vallée, Cedex 2, France

<sup>2</sup> Ankara University, Faculty of Engineering, Department of Chemical Engineering,  
06100 Tandogan, Ankara, Turkey

Corresponding author Email: [Mehmet.oturan@univ-eiffel.fr](mailto:Mehmet.oturan@univ-eiffel.fr)

# Graphical Abstract



## **Abstract**

The fast and complete removal of anti-cancer drug Cytarabine (CYT) from water was studied, for the first time, by electro-Fenton process using BDD anode and carbon felt cathode. A catalytic amount ( $10^{-4}$  M) of ferrous iron was initially added to the solution as catalyst and it was electrochemically regenerated in the process. Complete degradation of 0.1 mM ( $24.3 \text{ mg L}^{-1}$ ) CYT was achieved quickly in 15 min at 300 mA constant current electrolysis by hydroxyl radicals ( $\bullet\text{OH}$ ) electrocatalytically generated in the system. Almost complete mineralization (91.14% TOC removal) of the solution was obtained after 4 h of treatment. Mineralization current efficiency (MCE) and energy consumption (EC) during mineralization process were evaluated. The absolute (second order) rate constant for hydroxylation reaction of CYT by hydroxyl radicals was assessed by applying competition kinetics method and found to be  $5.35 \times 10^9 \text{ M}^{-1} \text{ s}^{-1}$ . Formation and evolution of oxidation reaction intermediates, short-chain carboxylic acids and inorganic ions were identified by gas chromatography-mass spectrometry, high performance liquid chromatography and ion chromatography analyses, respectively. Based on the identified intermediate and end-products, a plausible mineralization pathway for oxidation of CYT by hydroxyl radicals is proposed.

**Key Words:** Advanced oxidation processes; Electrochemical AOPs; Electro-Fenton; Cytarabine; Wastewater treatment

## 1. Introduction

Anti-cancer drugs are only partially metabolized and then discharged into sewage system from the hospitals and houses with the urine and/or feces of patients in the form of active substance and metabolites [1]. Cytarabine (CYT) is an anti-cancer drug which belongs to the category of antimetabolites [2]. It is an analogue of deoxycytidine and used to inhibit the growth of unregulated cancer cell by interfering with the DNA synthesis of the cell [3–5]. The urinary excretion rate for CYT is approximately 10% and its half-life degradation in human body is 1-3 h [6]. CYT has been detected in concentrations up to 9.2, 14, 13 ng L<sup>-1</sup> in influents and effluents of sewage treatment plants and surface waters, respectively [7]. These drugs cannot be successfully removed from water by conventional treatment methods due to their resistance to physical and biological treatments [8,9]. Therefore, effluents from wastewater treatment plants are considered to be the main source of release of anti-cancer drugs and their metabolites into the aquatic environment [10]. Chronic exposure to parent anti-cancer drugs and their transformation products are considered to be harmful to aquatic organisms and human due to their highly potent mechanism of action [10]. Therefore, it is of great importance to develop effective treatment methods to prevent the release of these drugs and their degradation intermediates to natural water media [11].

On the other hand, the advanced oxidation processes (AOPs) are becoming more and more important technologies for the efficient removal of non-biodegradable, persistent and toxic pollutants from water [12–15]. The main advantages of these processes are that they are relatively easy to operate due to the use of safe and environmentally friendly reagents, the absence of mass transfer restrictions and the short reaction time [16,17]. AOPs are based on the principle of in situ generation of strong oxidants, hydroxyl radicals (<sup>•</sup>OH) that can oxidize all type of organic pollutants in water [18,19]. Various AOP mechanisms have been proposed, and these mechanisms are classified depending on whether the hydroxyl radicals formation occurs: chemical, photochemical, sonochemical or electrochemical AOPs [12,20]. The oldest and most used AOP is the chemical Fenton process which is based on the use of a mixture of H<sub>2</sub>O<sub>2</sub> and ferrous iron to form hydroxyl radicals through Fenton reaction (Eq. (1)) [12].



34 This process presents some drawbacks such as external addition of reactants, risks  
 35 related to their transport and storage, and involvement of several wasting reactions  
 36 reducing process efficiency [21]. One of the ways to improve the Fenton process  
 37 efficiency is its combination with electrochemical technology [22]. Among the AOPs,  
 38 electrochemical advanced oxidation processes (EAOPs) are promising in terms of  
 39 industrial applicability with their advantages such as low operating cost [23,24] and  
 40 high removal efficiency of pollutants [25–27]. Electro-Fenton is one of the most popular  
 41 EAOPs for the removal of toxic and/or bio-refractory pollutants [28–30]. In this process,  
 42 H<sub>2</sub>O<sub>2</sub> is continuously electrogenerated at a suitable cathode by electro-reduction of O<sub>2</sub>  
 43 through the reaction given in Eq.(2) [31,32]. H<sub>2</sub>O<sub>2</sub> reacts with externally added catalyst  
 44 (Fe<sup>2+</sup>) to generate homogeneous hydroxyl radicals from Fenton's reaction (Eq. (1)) at  
 45 an optimal pH of around 3 [23,25]. Then, the catalyst Fe<sup>2+</sup> is continuously electro-  
 46 regenerated from reduction of Fe<sup>3+</sup> formed through Fenton reaction according to the  
 47 reaction given in Eq. (3) [33]. The continuous electrogeneration of H<sub>2</sub>O<sub>2</sub> and electro-  
 48 regeneration of Fe<sup>2+</sup> create a catalytic cycle accelerating oxidation/mineralization  
 49 processes [34].



52 The use of an anode material (M) with a high O<sub>2</sub> evolution overpotential such as BDD  
 53 electrode in electro-Fenton process allows the production of hydroxyl radicals at the  
 54 anode surface by water oxidation (Eq. (4)) [35,36]. These heterogeneously formed  
 55 radicals, noted M(<sup>•</sup>OH), are barely adsorbed on the electrode surface and behaves as  
 56 quasi free radicals in the vicinity of the anode [37]. Generation of these supplementary  
 57 hydroxyl radicals in the system enhances the efficiency of the process [38,39].



59 Electro-Fenton process is a promising method in terms of industrial applicability owing  
 60 to high pollutant removal efficiency and simple operating conditions [40]. Compared to  
 61 the classical Fenton process, the electro-Fenton process needs significantly less  
 62 amount of ferrous ion (as catalyst) [41,42]. In addition, H<sub>2</sub>O<sub>2</sub> is in situ generated in the

63 process [43]. The use of appropriate anode and cathode affects the efficiency of the  
64 process [44–46].

65 In this study, we investigated the kinetics of oxidation and mineralization of CYT  
66 solutions using electro-Fenton process with BDD anode and carbon felt cathode. To  
67 the best of our knowledge, this constitutes the first work on the efficient removal of CYT  
68 from contaminated water. We found only one report [3] treating anodic oxidation of  
69 CYT in which lower oxidation kinetics and mineralization rate were reported. The  
70 present study reports fast oxidative degradation kinetic (complete degradation in 15  
71 min) and almost complete mineralization (91.14% TOC removal at 4 h treatment).  
72 Besides, the reaction intermediates formed during the oxidation process, the short-  
73 chain carboxylic acids as final by-products before complete mineralization and mineral  
74 end-products were identified using HPLC, GC-MS and ion chromatography analysis  
75 methods. These data allowed to propose a plausible mineralization pathway of CYT  
76 by hydroxyl radicals generated in electro-Fenton process.

77

## 78 **2. Results and Discussion**

79

### 80 **2.1 Oxidative degradation kinetics of CYT**

81 Applied current is the key parameter controlling the regulation of the amounts of  
82 generated hydroxyl radicals through Eqs. (1-4) and therefore affecting the efficiency of  
83 electro-Fenton process [47,48]. Fig. 1a depicts the decay kinetics of CYT concentration  
84 when using BDD/carbon felt cell to elucidate the effect of current on degradation  
85 kinetics. As it can be seen in Fig. 1a, complete degradation of 0.1 mM CYT was quickly  
86 achieved in all cases, verifying that the drug is efficiently oxidized by hydroxyl radicals  
87 both in the bulk solution and at the surface of anode. Therefore, a second order  
88 reaction kinetics of CYT can be written as follows:



90

$$91 \frac{d[\text{CYT}]}{dt} = -k[\text{CYT}][\cdot\text{OH}] = -k_{app}[\text{CYT}] \quad (6)$$

92 where,  $k_{app}$  is the apparent rate constant. Since the electrolytic cell is operated under  
 93 galvanostatic conditions, hydroxyl radicals are produced at a constant rate in the  
 94 process and it is convenient to assume that they are consumed as soon as they are  
 95 produced. Thus, under these conditions, the second order reaction becomes a pseudo  
 96 first-order reaction. From the integration of Eq. (6), Eq. (7) is obtained as follows.

$$97 \ln \frac{[CYT]_0}{[CYT]_t} = k_{app} \times t \quad (7)$$

98 The slope of  $\ln([CYT]_0/[CYT]_t)$  versus  $t$  plot gives the  $k_{app}$  values [49] and results  
 99 obtained are given in Table 1 with coefficients of determination ( $R^2$ ) for CYT  
 100 degradation. According to the high values of  $R^2$  obtained in the experiments, it is  
 101 concluded that the pseudo-first order kinetics model for oxidation of CYT by hydroxyl  
 102 radicals generated in electro-Fenton process is described successfully.

103

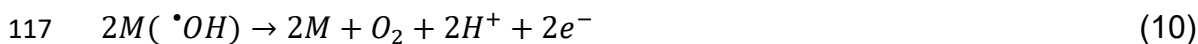
104 **Table 1.** Apparent rate constants for cytarabine (CYT) degradation by electro-Fenton

I (mA)	$k_{app}$ (min <sup>-1</sup> )	$R^2$
50	0.0825	0.9893
100	0.2367	0.9819
300	0.3616	0.9966
500	0.1688	0.9880

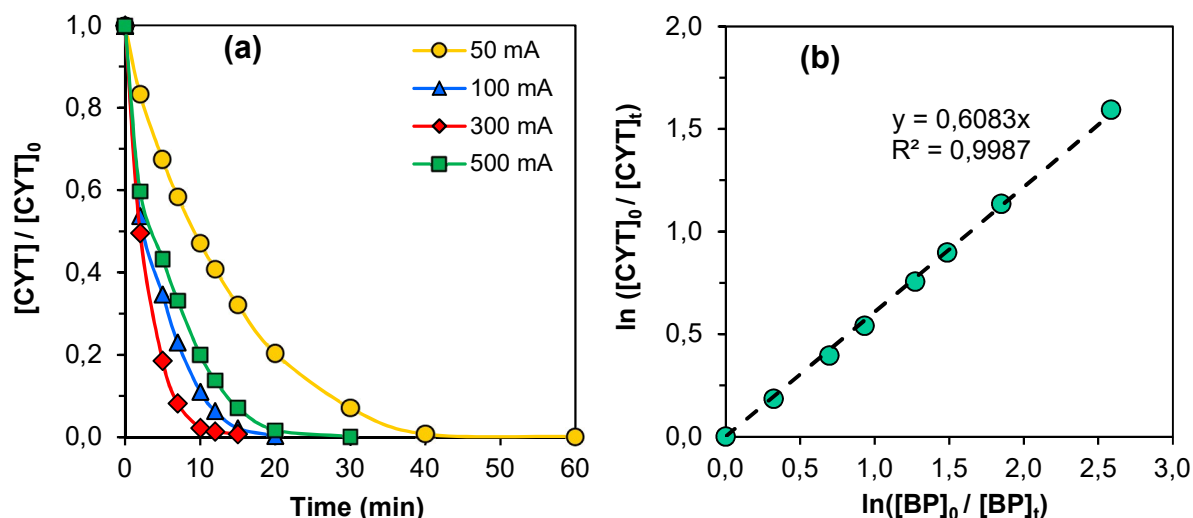
105

106 The decay of CYT concentration is improved by the increase in current value up to 300  
 107 mA for which complete degradation of CYT is achieved in 15 min. Further increase in  
 108 current value does not enhance the degradation efficiency. The decrease in the  
 109 oxidative degradation kinetic at high current values may be related to the enhancement  
 110 of the rate of the side reactions that inhibit the formation or promote the consumption  
 111 of hydroxyl radicals. The most important of these side reactions are (I) evolution of  $H_2$   
 112 at the cathode which competes with the formation of  $H_2O_2$  (Eq. (8)) and (II) evolution  
 113 of  $O_2$  in the bulk (Eq. (9)) and on the anode surface (Eq. (10)) which slow down the  
 114 oxidation rate [23,25].





118



119  
120 Fig. 1. Effect of current on CYT concentration decay (a) and determination of absolute  
121 rate constant ( $k_{CYT}$ ) of the reaction between CYT and hydroxyl radicals at 50 mA (b).  
122 Experimental conditions: pH = 3,  $[Na_2SO_4] = 50$  mM  $[Fe^{2+}] = 0.1$  mM

123

124 The absolute rate constant for hydroxylation reaction of CYT by hydroxyl radicals was  
125 assessed by applying competition kinetics method. This method is based on the  
126 competitive degradation of the target molecule and a standard competitor with a well-  
127 known rate constant [50]. Thus, benzophenone (BP) with absolute (second order) rate  
128 constant of  $k_{BP}$  of  $8.8 \times 10^9 \text{ M}^{-1} \text{ s}^{-1}$  was selected as standard competitor [51]. The  
129 absolute rate constant was then determined according to the Eq. (11):

130 
$$\ln\left(\frac{[CYT]_0}{[CYT]_t}\right) = \frac{k_{CYT}}{k_{BP}} \times \ln\left(\frac{[BP]_0}{[BP]_t}\right)$$
 (11)

131 Here,  $k_{CYT}$  and  $k_{BP}$  are the absolute rate constants for oxidation reaction by hydroxyl  
132 radicals for CYT and benzophenone, respectively. In order to avoid the interference of  
133 the oxidation products, experiments were performed at 50 mA and on a short  
134 electrolysis time. A solution containing the same concentration (0.1 mM) of both CYT  
135 and benzophenone was oxidatively degraded in presence of 0.1 mM  $Fe^{2+}$  at pH 3, and  
136  $k_{CYT}$  was then calculated as  $5.35 \times 10^9 \text{ M}^{-1} \text{ s}^{-1}$  from the slope of the line given in Fig. 1b.

137

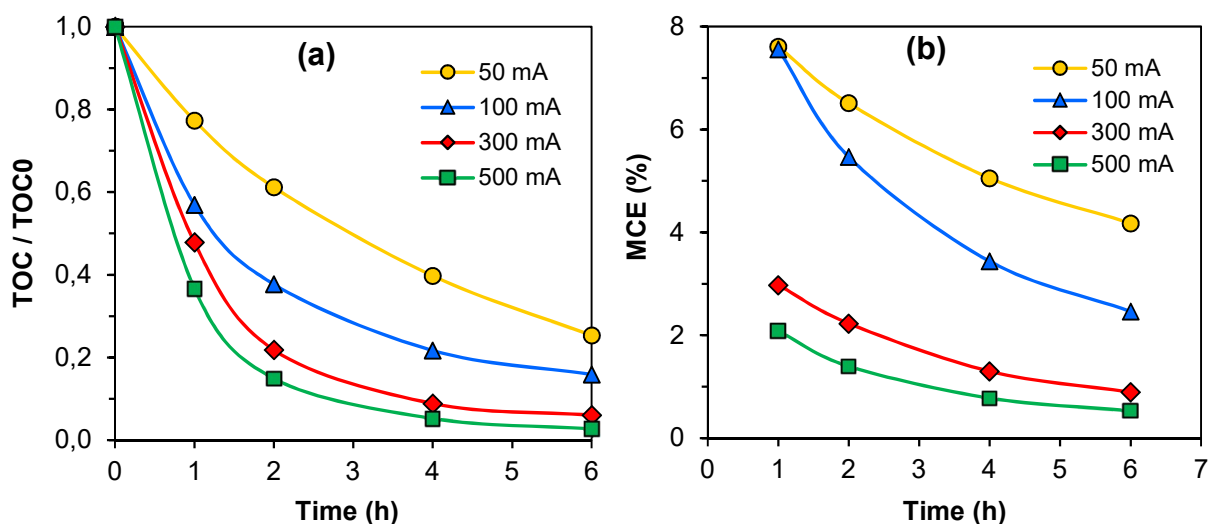
138 **2.2 Mineralization of CYT aqueous solution**

139 The complete oxidative degradation of the target pollutant does not mean that the  
140 solution to be treated is cleaned effectively due to the generation of intermediate  
141 products which can be more toxic or refractory compared to mother molecule [52]. For  
142 an effective treatment, almost total removal of mother pollutants and their oxidation  
143 intermediates are required. Hence, the mineralization of 0.1 mM CYT solution was  
144 performed at different current values with regard to TOC removal efficiency. As it can  
145 be seen from Fig. 2a, TOC removal rate increases with the increments of current from  
146 50 to 500 mA, as expected from the enhanced production of hydroxyl radicals. This  
147 fact can be explained by the high of oxygen evolution overpotential of BDD anode  
148 allowing the formation of high amount of heterogeneously formed hydroxyl radicals  
149 (Eq. (4)) as well as homogeneously formed hydroxyl radicals in the bulk due to the  
150 increased rate of electrogenerated  $H_2O_2$  and fast electro-regeneration of  $Fe^{2+}$ ,  
151 promoting Fenton's reaction (Eqs. (1) – (3)) [53,54]. According to Fig. 2a, the  
152 percentage TOC removal after 4 h treatment was observed as 91.14 and 94.77% at  
153 300 mA and 500 mA, respectively, showing that almost complete mineralization is  
154 achieved. When increasing applied current value, the difference in TOC decay rate  
155 observed at lower current values is greater than that observed between higher  
156 currents. This behavior can be explained by acceleration of parasitic non-oxidative  
157 reactions of hydroxyl radicals at higher current values, mainly heterogeneously formed  
158 hydroxyl radicals oxidation to  $O_2$  (Eq. (10)) and recombination of homogeneously  
159 formed hydroxyl radicals to  $H_2O_2$  (Eqs. (12) and (13)). It is also observed that TOC  
160 shows a very sharp decay during the first two hours of electrolysis followed by a much  
161 slower removal rate. This phenomenon can be explained by the loss of organic matter  
162 in the solution on the one hand and the formation of more recalcitrant organic  
163 compounds such as short-chain carboxylic acids on the other hand [54–56].



166

167



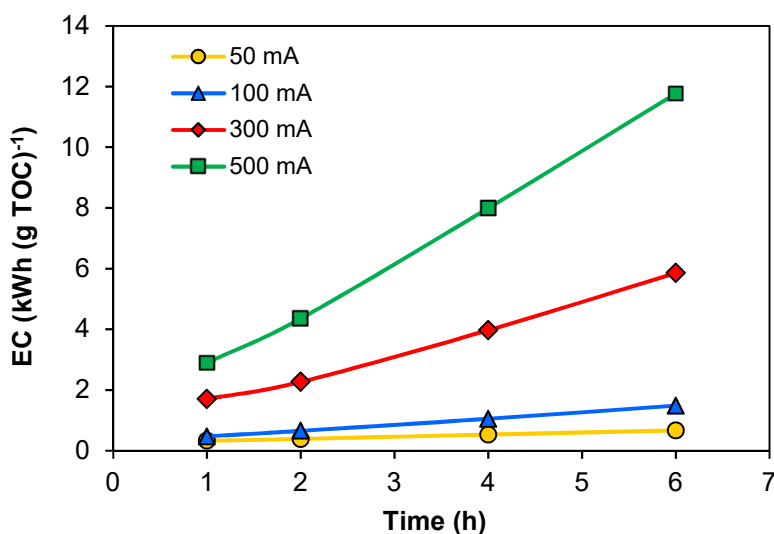
168  
 169 **Fig. 2.** Effect of current on normalized TOC removal of 0.1 mM CYT in 50 mM Na<sub>2</sub>SO<sub>4</sub>  
 170 solution containing 0.1 mM Fe<sup>2+</sup> (a) and evolution of MCE during time (b). Experimental  
 171 conditions: pH = 3 in, [Na<sub>2</sub>SO<sub>4</sub>] = 50 mM, [Fe<sup>2+</sup>] = 0.1 mM  
 172

173 Fig. 2b represents the mineralization current efficiency (MCE) values that reflects the  
 174 proportion of the current used for mineralization of CYT. The MCE curves are getting  
 175 closer with the increase in current as in TOC decay. It is observed that MCE  
 176 progressively decays after showing a maximum value at the beginning of electrolysis,  
 177 suggesting the loss of organic matter and the generation of persistent by products  
 178 (such as short-chain carboxylic acids) occurring just after the rapid oxidation of  
 179 organics under the attack of hydroxyl radicals. After 6 h of electrolysis, MCE values  
 180 were 4.17, 2.46, 0.89 and 0.53 % for 50, 100, 300 and 500 mA current intensities,  
 181 respectively. This can be clarified by the enhancement of the rate of waste reactions  
 182 that consume hydroxyl radicals or electrical energy spent for generation of less  
 183 powerful oxidation species in side reactions, such as H<sub>2</sub> evolution at the cathode and  
 184 O<sub>2</sub> evolution at the anode [57] as detailed above.

185 The MCE is an important parameter in view of large application of a process. In  
 186 general, the depletion of MCE has been reported to be associated with an increase of  
 187 the energy consumption (EC) per unit TOC removed [17]. Evolution of EC for current  
 188 values ranging from 50 to 500 mA was shown in Fig. 3 to evaluate the cost  
 189 effectiveness of the process. According to the results, higher current and longer  
 190 electrolysis time result in high EC. The increase in allied current enhances the  
 191 mineralization of organic pollutants up to a maximum value followed by a decrease due

192 to the acceleration of non-oxidizable parasitic reactions and generation of recalcitrant  
193 intermediates as discussed above.

194



195

196 **Fig. 3.** Evolution of EC during the electrolysis of 0.1 mM CYT in 50 mM of Na<sub>2</sub>SO<sub>4</sub>  
197 solution containing 0.1 mM Fe<sup>2+</sup> as a function of current

198

### 199 2.3 Formation and evolution of carboxylic acids and inorganic ions

200 The oxidative degradation of organic pollutants by hydroxyl radicals lead to the  
201 formation of a variety of short-chain carboxylic acids, which are the lowest molecular  
202 weight organic species and ultimate reaction intermediates before total mineralization  
203 step consisting of transformation to CO<sub>2</sub>, H<sub>2</sub>O and inorganic ions during AOPs [23,54].

204 These species are reported to be less reactive against the attack of hydroxyl radicals  
205 and generally need longer electrolysis times for complete mineralization [58,59]. The

206 identification and evolution of carboxylic acids during mineralization of CYT in electro-  
207 Fenton process were shown in Fig. 4a. Ion-exclusion chromatograms allowed the

208 detection of four carboxylic acids with well-defined peaks corresponding to oxalic,  
209 oxamic, pyruvic and formic acids at retention times (t<sub>R</sub>) of 6.64, 9.87, 11.28, 13.55 min,

210 respectively. The concentration profile of these carboxylic acids follows a quick  
211 accumulation trend at the early stage of the electrochemical treatment with regard to

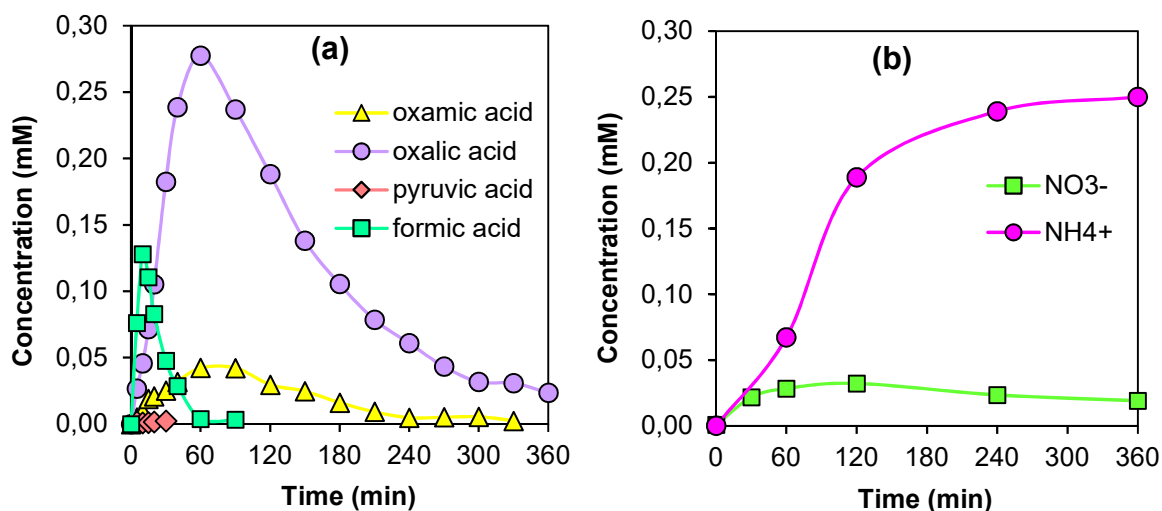
212 quick oxidation of target molecule and its organic cyclic intermediates by  
213 electrogenerated hydroxyl radicals [60]. However, the concentration of these species

214 gradually decreased with the electrolysis time since they are present in the medium  
215 mainly as Fe(III)-carboxylate complexes which require longer destruction times due to

216 their lower reactivity with hydroxyl radicals [49,53]. As seen from Fig. 4a, pyruvic acid  
217 was detected at trace level and disappeared in about 30 min electrolysis. Oxalic acid  
218 which is regarded as the ultimate end product before total mineralization [61,62] was  
219 obtained at maximum concentration (0.28 mM) at 60 min. In addition, formic and  
220 oxamic acids reached maximum values at 10 and 60 min, respectively. It can be noted  
221 that these two carboxylic acids were completely removed in 90 and 330 min of  
222 electrolysis, respectively, whereas the concentration of oxalic acid was slowly  
223 decreased to a low amount (0.023 mM) during electrolysis with BDD anode. This is  
224 consistent with low TOC values under the same experimental conditions presented in  
225 sub-section 3.2.

226 The heteroatoms in the structure of organic molecules are oxidized to inorganic ions  
227 that are released in the solution during mineralization. The identification and evolution  
228 of inorganic ions (corresponding to heteroatoms in the structure of mother organic  
229 pollutant) represent another important indicator for mineralization of organic pollutants  
230 [54,56]. CYT contains three N atoms in its initial structure which expected to be  
231 mineralized into inorganic ions  $\text{NO}_3^-$  and  $\text{NH}_4^+$  upon cleavage of the covalent bonds in  
232 the molecule. Inorganic ions formed during the mineralization of 0.1 mM CYT solution  
233 were identified and quantified by ion chromatography. The evolution of  $\text{NO}_3^-$  and  $\text{NH}_4^+$   
234 was depicted in Fig. 4b while  $\text{NO}_2^-$  ion was not detected in the solution. It can be seen  
235 that the concentration of  $\text{NH}_4^+$  ion which continuously accumulated along with the  
236 electrolysis time is significantly higher than that of  $\text{NO}_3^-$  in the solution. At the early  
237 stages of the electrolysis, concentration of  $\text{NH}_4^+$  increased with treatment time and  
238 gradually reached to a plateau. The concentration of  $\text{NO}_3^-$  remained almost constant  
239 after 1 h electrolysis can be related to its reduction to  $\text{NH}_4^+$  ion on the carbon felt  
240 cathode in agreement with previous reports [58,63]. After 6 h of electrolysis, the  
241 concentration of  $\text{NH}_4^+$  ion in the final solution was determined as 0.250 mM (83.3 % of  
242 initial N) whereas the concentration of  $\text{NO}_3^-$  was 0.019 mM (6.3 % of initial N). The  
243 sum of these two inorganic ions released in the solution was calculated as 0.27 mM  
244 representing 90% of the total nitrogen content in initial solution. The slight loss of N  
245 could be explained with the generation of gaseous nitrogen compounds ( $\text{N}_2$ ,  $\text{N}_2\text{O}_5$ ,  
246  $\text{NO}_x$ ) via the cathodic reduction of  $\text{NO}_3^-$  [64].

247



248  
249

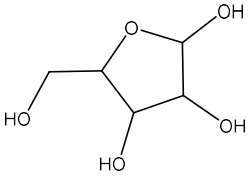
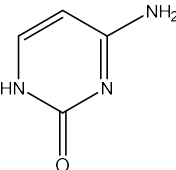
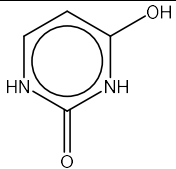
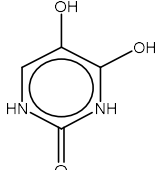
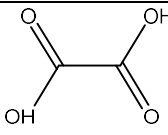
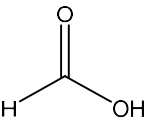
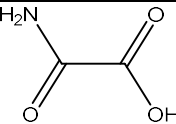
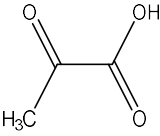
250 **Fig. 4.** Evolution of short-chain carboxylic acids **(a)** and inorganic ions **(b)** during  
251 electrolysis of 0.1 mM CYT solution containing 0.1 mM Fe<sup>2+</sup> (as catalyst) during electro-  
252 Fenton treatment with BDD anode and carbon-felt cathode at pH=3. Applied current  
253 was 100 mA for carboxylic acids whereas it was 300 mA for inorganic ions. The  
254 concentration of the supporting electrolyte (Na<sub>2</sub>SO<sub>4</sub>) was 50 mM for carboxylic acids  
255 while it was 15 mM for inorganic ions to avoid the interference of Na<sup>+</sup> ions on analysis.

## 256 2.4 Mineralization pathway for CYT

257 The identification of the aromatic oxidation products formed during electro-Fenton  
258 treatment was performed using GC-MS analysis (Table 2). These data combined to  
259 those related to carboxylic acids and inorganic end-products (detailed in sub-section  
260 2.3) allowed proposing a plausible mineralization pathway of CYT by hydroxyl radicals  
261 generated during the electro-Fenton process (Table 2, Fig. 5). The intermediates I to  
262 IV were identified thanks to the fragmentation analysis of GC-MS spectrum while the  
263 intermediates V to VIII were identified by ion-exclusion HPLC analysis. The proposed  
264 pathway starts by the attack of hydroxyl radicals on CYT leading to oxidative cleavage  
265 into molecules I (D-ribofuranose) and II (cytosine). Compounds III and IV were resulted  
266 of hydroxylation of cytosine. Further attacks of hydroxyl radicals causes oxidative ring  
267 opening reactions of these aromatic structure leading to the formation of carboxylic  
268 acids (compounds V to VIII) and inorganic ions through deamination and  
269 decarboxylation mechanisms. Mineralization of the carboxylic acids to CO<sub>2</sub>, water and  
270 inorganic ions constitutes the last stage of mineralization in agreement with TOC and  
271 inorganic ions analysis.

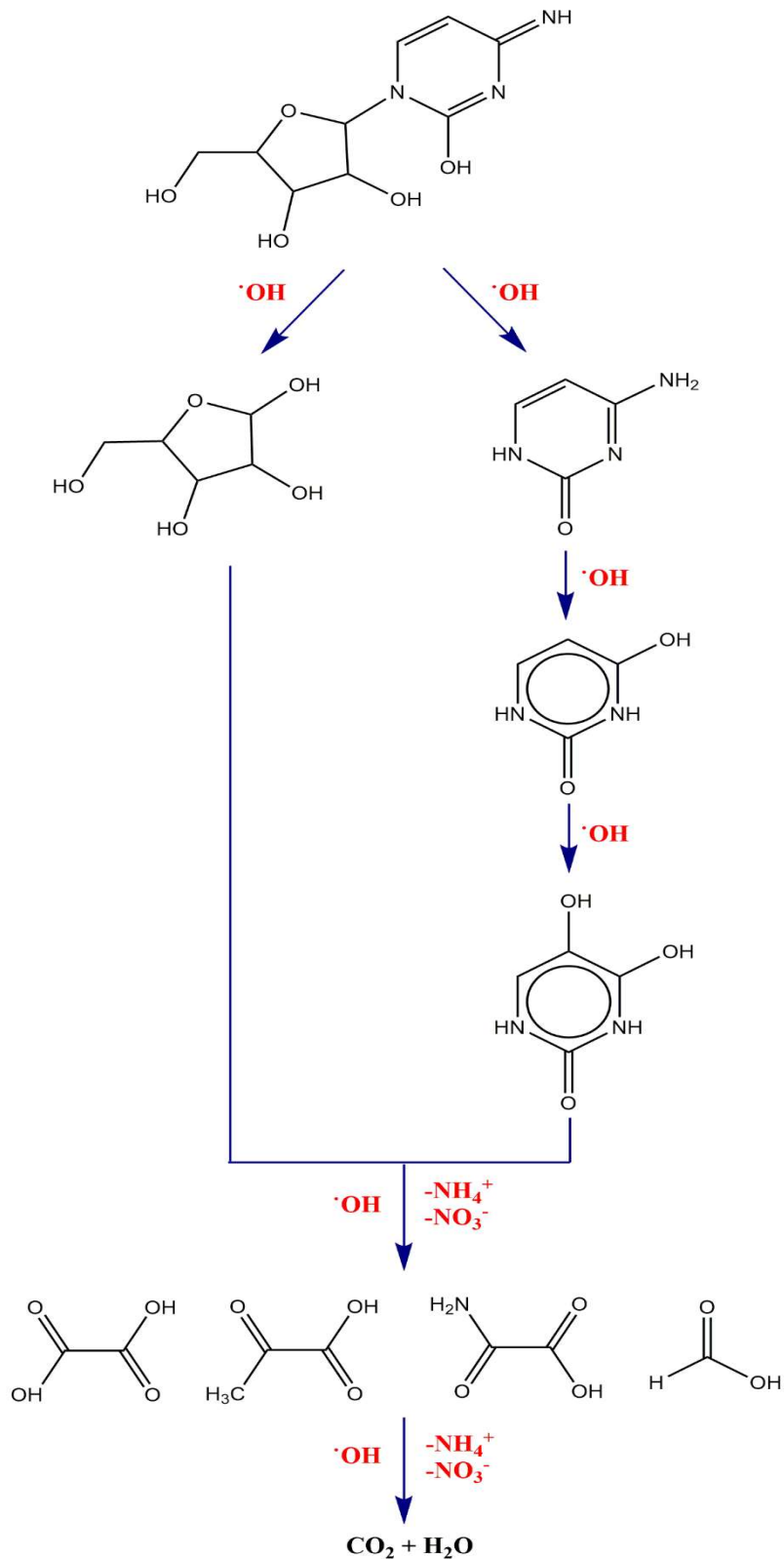
272

273 **Table 2.** Intermediate products identified using GC-MS and HPLC during the  
 274 mineralization of CYT by electro-Fenton process with BDD anode

Compound #	Molecular mass (g mol <sup>-1</sup> )	Retention time (min)	Molecular structure	Analytical technique
I	150	13.46		GC-MS
II	111	20.07		GC-MS
III	113	23.58		GC-MS
IV	129	19.96		GC-MS
V	90	6.64		HPLC
VI	46	13.55		HPLC
VII	89	9.87		HPLC
VIII	88	11.28		HPLC

275

276



277

278 **Fig. 5.** Proposed reaction pathway for mineralization of CYT by hydroxyl radicals based  
 279 on TOC data and identified oxidation intermediates, short-chain carboxylic acids and  
 280 mineral end-products

281

## 282 **3. Material and Methods**

283

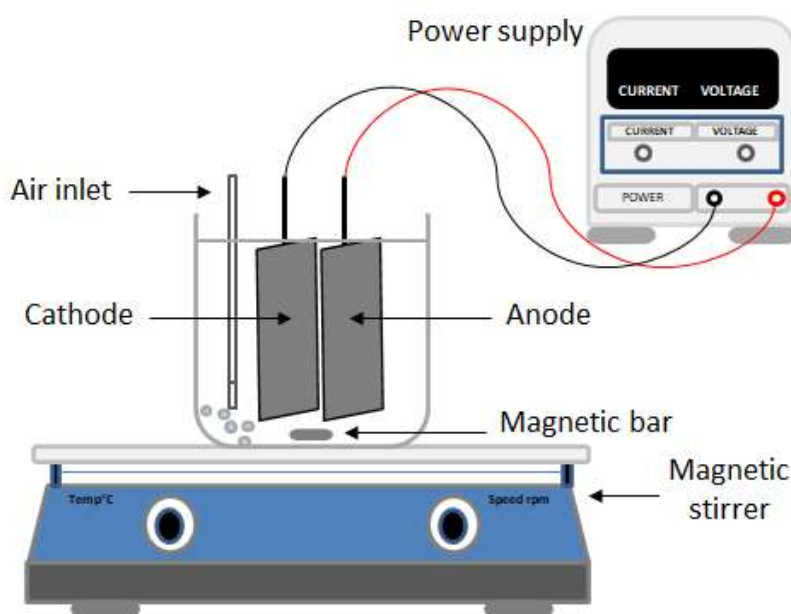
### 284 **3.1 Chemicals**

285 CYT, C<sub>9</sub>H<sub>13</sub>N<sub>3</sub>O<sub>5</sub>, with purity >98%, was purchased from Acros Organics and was used  
286 without further purification. Methanol and phosphoric acid (H<sub>3</sub>PO<sub>4</sub>) used in the  
287 preparation of HPLC eluents were supplied by Sigma-Aldrich and Fluka, respectively.  
288 Sodium sulfate (Na<sub>2</sub>SO<sub>4</sub> ≥ 99% purity) used as supporting electrolyte and iron (II)  
289 sulphate heptahydrate (FeSO<sub>4</sub>·7H<sub>2</sub>O ≥ 99.5% purity) used as source of the catalyst  
290 were provided by Merck and Sigma-Aldrich, respectively. Sulfuric acid (H<sub>2</sub>SO<sub>4</sub>) and  
291 sodium hydroxide (NaOH) used to adjust solution pH were of analytical grade from  
292 Acros Organics and Fluka, respectively. HPLC eluents and CYT working solutions  
293 were prepared with ultra-pure water obtained from a Millipore Milli-Q system with  
294 resistivity > 18 MΩ cm at 25 °C. Organic solvents and other chemicals used were either  
295 HPLC or analytic grade from Sigma-Aldrich. Oxalic (C<sub>2</sub>H<sub>2</sub>O<sub>4</sub>), oxamic (C<sub>2</sub>H<sub>3</sub>NO<sub>3</sub>),  
296 pyruvic (C<sub>3</sub>H<sub>4</sub>O<sub>3</sub>) and formic (CH<sub>2</sub>O<sub>2</sub>) acids used as standards for quantifying short-  
297 chain aliphatic carboxylic acids generated during electro-Fenton treatment were  
298 obtained from Acros Organics, Fluka and Alfa Aesar.

### 299 **3.2 Electrolytic system**

300 Homogeneous electro-Fenton experiments were performed in a 250 mL undivided  
301 cylindrical glass cell. To homogenize the solution, a magnetic stirrer and compressed  
302 air bubbling were used. The bubbling was started 5 min before the beginning of the  
303 experiment to provide saturated oxygen condition in the solution for H<sub>2</sub>O<sub>2</sub> generation.  
304 BDD film on niobium support (CONDIAS GmbH, Germany) was used as anode and  
305 unmodified 3D carbon felt electrode (MERSEN, France) was used as cathode. Both  
306 electrodes had the surface area of 4 x 8 cm<sup>2</sup>. Experiments were carried out at room  
307 temperature and at pH 3. This value is well established to be optimal for Fenton  
308 process and all related processes including electro-Fenton process [12, 23, 30]. The  
309 pH was measured with a CyberScan pH 1500 pH-meter from Eutech Instruments. The  
310 electrochemical cell was powered by a Hameg HM8040 triple DC power supply. A  
311 schematic illustration of the electrochemical experimental system is presented in Fig.  
312 6. Experiments were performed under constant current electrolysis conditions ranging  
313 from 50 mA to 500 mA. 220 mL aqueous solution containing 0.1 mM CYT as target

314 pollutant, 0.1 mM Fe<sup>2+</sup> as catalyst. Electrolysis were performed in 50 mM Na<sub>2</sub>SO<sub>4</sub> as  
315 supporting electrolyte since it behaves as inert under electro-Fenton conditions. 50 mM  
316 is enough to provide a conductivity for the passage of current without loss of electrical  
317 energy [12, 23]. . Samples were taken during electrolysis at pre-set time intervals in  
318 order to evaluate the concentration for decay kinetics of CYT, mineralization rate,  
319 carboxylic acids evolution and inorganic ions released. All experiments for degradation  
320 kinetics and TOC abatement were performed at least twice and the mean values are  
321 reported on the figures.



322

323 Fig. 6. Schematic illustration of electrolytic system used in this work

324

### 325 3.3 Analytical procedures

326 The CYT concentration is measured by HPLC using a Merck Lachrom Liquid  
327 chromatography system equipped with a quaternary pump L-7100, fitted with a  
328 Purospher RP 18, 5 μm, 25 cm×4.6 mm (i.d.) column from VWR International  
329 (Fontenay-sous-Bois, France) at 40°C and coupled with a L-7455 diode array detector  
330 from Hitachi (Fontenay-sous-Bois, France). The analysis of CYT is carried out with a  
331 mobile phase composed of methanol/water (with 0.4% phosphoric acid) 2:98 (v/v)  
332 mixture in isocratic elution mode at a flow rate of 0.3 mL min<sup>-1</sup>. The detection was  
333 performed at the wavelength of 271 nm. Samples of 20 μL were injected into the  
334 system and measurements were controlled through EZ-Chrom Elite 3.1 software.

335 The extent of mineralization during the treatment of CYT was monitored from the  
 336 abatement of their total organic carbon (TOC) value using a Shimadzu TOC-V<sub>CSH</sub>  
 337 analyzer according to the thermal catalytic oxidation principle. The carrier gas was  
 338 oxygen with a flow rate of 150 mL min<sup>-1</sup>. The temperature in the oven was 680 °C.  
 339 Platinum was used as catalyst in order to carry out the total combustion reaction at this  
 340 temperature. Calibration of the analyzer was done with potassium hydrogen phthalate  
 341 standard. Reproducible TOC values are obtained using the non-purgeable organic  
 342 carbon method with an accuracy of ± 2% by injecting 50 µL aliquots into the analyzer.  
 343 TOC values were also utilized for determination of mineralization current efficiency  
 344 (MCE) and energy consumption (EC). MCE was calculated according to the following  
 345 equation (Eq. (14)) [14]:

$$346 \quad MCE(\%) = \frac{n F V_S \Delta(TOC)_{exp}}{4.32 \times 10^7 m I t} \times 100 \quad (14) \text{Here } F$$

347 is the Faraday constant (96485 C mol<sup>-1</sup>), V<sub>S</sub> is the solution volume (L), Δ(TOC)<sub>exp</sub> is the  
 348 experimental TOC decay (mg L<sup>-1</sup>), 4.32 × 10<sup>7</sup> is a conversion factor for homogenization  
 349 of units, m is the number of carbon atoms of CYT, I is applied current (A), t is the  
 350 electrolysis time (h). n is the number of electrons consumed per CYT molecule during  
 351 mineralization and was taken as 30 with the assumption of transformation of the N  
 352 atoms in CYT molecule into NH<sub>4</sub><sup>+</sup> according to the mineralization reaction (Eq. (15)).



354 EC was calculated by using Eq. (16) [23]:

$$355 \quad EC(kWh(g TOC)^{-1}) = \frac{E_{cell} I t}{V_S \Delta(TOC)_{exp}} \quad (16)$$

356 where E<sub>cell</sub> is the mean potential difference of the cell (V).

357 The evolution of the short-chain carboxylic acids generated during electro-Fenton  
 358 treatment as the final organic by-products of the mineralization process were identified  
 359 and quantified by the same HPLC equipped with a Biorad column (9 mm, 250 mm, 4.6  
 360 mm) coupled with a UV detector set to 220 nm. 4 mM H<sub>2</sub>SO<sub>4</sub> was used as mobile  
 361 phase in isocratic elution mode with a flow rate of 0.6 mL min<sup>-1</sup>. For identification and  
 362 quantification of carboxylic acids, comparison of the retention time and peak area of  
 363 standard solutions were performed.

364 Inorganic ions,  $\text{NO}_3^-$  and  $\text{NH}_4^+$ , released in the solution during mineralization of CYT  
365 were identified and quantified by Dionex ICS-1000 Basic Ion Chromatography System  
366 coupled with a Dionex DS6 conductivity detector containing a cell maintained at  $35^\circ\text{C}$ .  
367 The data acquisition was done by Chromeleon software. The  $\text{NH}_4^+$  content was  
368 detected and measured with a Dionex CS12A,  $25\text{ cm} \times 4\text{ mm}$  (i.d.) cationic column  
369 and a mobile phase of  $30\text{ mM}$  methanesulfonic acid at  $0.36\text{ mL min}^{-1}$ , whereas the  
370  $\text{NO}_3^-$  content was measured with a Dionex AS4A-SC,  $25\text{ cm} \times 4\text{ mm}$  (i.d.) anionic  
371 column and a mobile phase as a mixture of  $1.8\text{ mM Na}_2\text{CO}_3$  and  $1.7\text{ mM NaHCO}_3$   
372 solution at  $1.2\text{ mL min}^{-1}$ . The applied current in the suppressor SRS (Self Regenerating  
373 Suppressor) that is required to prevent the effect of the eluent ions in the detector  
374 signal was  $30\text{ mA}$  in both cases.

375 In order to identify the cyclic/aromatic intermediates formed during electro-Fenton  
376 treatment,  $0.1\text{ mM}$  CYT solution was electrolyzed at  $50\text{ mA}$  during  $30\text{ min}$ . Samples for  
377 GC-MS were obtained by solvent extraction of organic components. Extraction of  
378 resulting organics was performed three times with ethyl acetate followed by  
379 evaporation of the solution. Then the organic fraction were again diluted with the same  
380 organic solvent. GC-MS analyses were performed using a Thermo Scientific GC-MS  
381 analyzer equipped with TRACE 1300 gas chromatography coupled to an ISQ single  
382 quadrupole mass spectrophotometer operating in electron impact mode at  $70\text{ eV}$ .  
383 Samples were injected to GC-MS using a TG-5Ms  $0.25\text{ mm}$ ,  $30\text{ m}$ ,  $0.25\text{ mm}$  (i.d.)  
384 column. The temperature ramp for this column was applied as  $50^\circ\text{C}$  during  $1\text{ min}$ ,  $10$   
385  $^\circ\text{C min}^{-1}$  to  $330^\circ\text{C}$  and kept at this temperature for  $5\text{ min}$ . The temperature of the inlet  
386 and detector were  $200$  and  $250^\circ\text{C}$ , respectively. Helium was used as carrier gas at a  
387 flow rate of  $1.2\text{ mL min}^{-1}$ .

#### 388 **4. Conclusions**

389 According to the results obtained in the degradation kinetics studies, complete  
390 oxidative degradation of  $0.1\text{ mM}$  ( $24.32\text{ mg L}^{-1}$ ) CYT was achieved at  $15\text{ min}$  under  
391  $300\text{ mA}$  at  $\text{pH } 3$  using electro-Fenton process with BDD/carbon felt electrode cell.  
392 Almost complete mineralization ( $97\%$  of total organic carbon removal) of the same  
393 solution was obtained after  $360\text{ min}$  under  $500\text{ mA}$  constant current. The absolute rate  
394 constant of oxidation reaction of CYT by hydroxyl radicals was determined using  
395 competition kinetic method and found to be  $5.35 \times 10^9\text{ M}^{-1}\text{ s}^{-1}$ . A literature survey was

396 carried out in order to compare the degradation/mineralization performance of the  
 397 electro-Fenton process with previously published studies on the treatment of CYT.  
 398 These data are summarized below in Table 3. As can be observed, the CYT  
 399 degradation by electro-Fenton process seems to be more efficient than other strategies  
 400 in terms of total degradation rate and mineralization efficiency.

401

402 Table 3. Degradation/mineralization performance of CYT with various methods

Method	Experimental Conditions	Removal (%)	Reference
UV/H <sub>2</sub> O <sub>2</sub>	[CYT] <sub>0</sub> =10 mg/L [H <sub>2</sub> O <sub>2</sub> ]=400µM pH=7	90% degradation in 120 min	[65]
UV/K <sub>2</sub> S <sub>2</sub> O <sub>8</sub>	[CYT] <sub>0</sub> =10 mg/L [K <sub>2</sub> S <sub>2</sub> O <sub>8</sub> ]=200µM pH=7	98% degradation in 60 min	[65]
Gamma Radiation	[CYT] <sub>0</sub> =10 mg/L Dose rate = 1.66 Gy min <sup>-1</sup> pH=7	95% degradation in 240 min	[66]
UV/TiO <sub>2</sub> + Activated Carbon	[CYT] <sub>0</sub> =50 mg/L Carbon mass = 5 mg TiO <sub>2</sub> mass =5 mg pH=7	90% degradation in 10 min	[67]
Photodegradation	[CYT] <sub>0</sub> =10 mg/L [K <sub>2</sub> S <sub>2</sub> O <sub>8</sub> ]=100µM pH=7	90% degradation in 30 min 45% mineralization in 120 min	[68]
Simulated Solar Photocatalysis	[CYT] <sub>0</sub> =30 mg/L [TiO <sub>2</sub> ]= 300 mg/L [H <sub>2</sub> O <sub>2</sub> ]=90 mg/L pH=6.5	100% degradation in 30 min 80% mineralization in 360 min	[7]
Photo-Fenton-like treatment	[CYT] <sub>0</sub> =30 mg/L [Fe <sup>3+</sup> ]= 3 mg/L	100% degradation in 30 min	[6]

	[C <sub>2</sub> K <sub>2</sub> O <sub>4</sub> ·H <sub>2</sub> O]= 90 mg/L pH=3	82% mineralization in 360 min	
Anodic oxidation	[CYT] <sub>0</sub> =20 mg L <sup>-1</sup> Graphite anode Current density = 10 mA cm <sup>-2</sup> [NaCl]= 50 mM pH=3	98% degradation in 30 min 60% mineralization in 180 min	[3]
<b>Electro-Fenton (Present work)</b>	[CYT] <sub>0</sub> =24.32 mgL <sup>-1</sup> BDD anode Carbon felt cathode [Na <sub>2</sub> SO <sub>4</sub> ]= 50 mM pH=3	100% degradation in 15 min 91% mineralization in 240 min at 300 mA (9.375 mA cm <sup>-2</sup> ) 85% mineralization in 120 min at 500 mA (15.625 mA cm <sup>-2</sup> ) 95% mineralization in 240 min at 500 mA (15.625 mA cm <sup>-2</sup> )	This study

403

404

**Author Contributions:**

S.C.: Conceptualization, Investigation, Methodology, Draft preparation, Writing, Formal analysis.

B.Ö.: Investigation, Validation, Writing

N.O.: Supervision, Methodology, Formal analysis

C.T.: Supervision, Validation

M.A.O.: Supervision, Review & editing, Project administration

**Funding:** This research received no external funding.

**Institutional Review Board Statement:** Not applicable.

**Informed Consent Statement:** Not applicable.

**Data Availability Statement:** Data is contained within the article.

**Acknowledgments:** Sule Camcioglu and Baran Ozyurt acknowledge TUBITAK (The Scientific and Technological Research Council of Turkey) for providing financial support through 2219-International Postdoctoral Research Fellowship Program for Turkish Citizens. Sule Camcioglu and Baran Özyurt thank both Ankara University and Gustave Eiffel University for their support of their postdoctoral research.

**Conflicts of Interest:** The authors declare no conflict of interest.

## References

1. Zhang, J.; Chang, V.W.C.; Giannis, A.; Wang, J.-Y. Removal of cytostatic drugs from aquatic environment: a review. *Sci. Total Environ.* **2013**, *445*, 281–298.
2. Besse, J.-P.; Latour, J.-F.; Garric, J. Anticancer drugs in surface waters: what can we say about the occurrence and environmental significance of cytotoxic, cytostatic and endocrine therapy drugs? *Environ. Int.* **2012**, *39*, 73–86.
3. Sivodia, C.; Sinha, A. Assessment of graphite electrode on the removal of anticancer drug cytarabine via indirect electrochemical oxidation process: Kinetics & pathway study. *Chemosphere* **2020**, *243*, 125456.
4. Espinosa, E.; Zamora, P.; Feliu, J.; Barón, M.G. Classification of anticancer drugs—a new system based on therapeutic targets. *Cancer Treat. Rev.* **2003**, *29*, 515–523.
5. Herold, N.; Rudd, S.G.; Ljungblad, L.; Sanjiv, K.; Myrberg, I.H.; Paulin, C.B.J.; Heshmati, Y.; Hagenkort, A.; Kutzner, J.; Page, B.D.G. Targeting SAMHD1 with the Vpx protein to improve cytarabine therapy for hematological malignancies. *Nat. Med.* **2017**, *23*, 256–263.
6. Koltsakidou, A.; Antonopoulou, M.; Evgenidou, E.; Konstantinou, I.; Lambropoulou, D. A comparative study on the photo-catalytic degradation of Cytarabine anticancer drug under Fe<sup>3+</sup>/H<sub>2</sub>O<sub>2</sub>, Fe<sup>3+</sup>/S<sub>2</sub>O<sub>8</sub><sup>2-</sup>, and [Fe (C<sub>2</sub>O<sub>4</sub>)<sub>3</sub>]<sup>3-</sup>/H<sub>2</sub>O<sub>2</sub> processes. Kinetics, identification, and in silico toxicity assessment of generated transformation products. *Environ. Sci. Pollut. Res.* **2019**, *26*, 7772–7784.
7. Koltsakidou, A.; Antonopoulou, M.; Evgenidou, E.; Konstantinou, I.; Lambropoulou, D.A. Cytarabine degradation by simulated solar assisted photocatalysis using TiO<sub>2</sub>. *Chem. Eng. J.* **2017**, *316*, 823–831.
8. Booker, V.; Halsall, C.; Llewellyn, N.; Johnson, A.; Williams, R. Prioritising anticancer drugs for environmental monitoring and risk assessment purposes. *Sci. Total Environ.* **2014**, *473*, 159–170.
9. Pieczyńska, A.; Fiszka Borzyszkowska, A.; Ofiarska, A.; Siedlecka, E.M. Removal of cytostatic drugs by AOPs: A review of applied processes in the context of green technology. *Crit. Rev. Environ. Sci. Technol.* **2017**, *47*, 1282–1335.
10. Santana-Viera, S.; Montesdeoca-Esponda, S.; Sosa-Ferrera, Z.; Santana-Rodríguez, J.J. Cytostatic drugs in environmental samples: An update on the extraction and determination procedures. *TrAC Trends Anal. Chem.* **2016**, *80*, 373–386.
11. Siedlecka, E.M.; Ofiarska, A.; Borzyszkowska, A.F.; Białk-Bielińska, A.; Stepnowski, P.; Pieczyńska, A. Cytostatic drug removal using electrochemical oxidation with BDD electrode: degradation pathway and toxicity. *Water Res.* **2018**, *144*, 235–245.
12. Oturan, M.A.; Aaron, J.-J. Advanced oxidation processes in water/wastewater

- treatment: principles and applications. A review. *Crit. Rev. Environ. Sci. Technol.* **2014**, *44*, 2577–2641.
13. Poza-Nogueiras, V.; Rosales, E.; Pazos, M.; Sanroman, M.A. Current advances and trends in electro-Fenton process using heterogeneous catalysts—a review. *Chemosphere* **2018**, *201*, 399–416.
  14. Ganiyu, S.O.; Sable, S.; El-Din, M.G. Advanced oxidation processes for the degradation of dissolved organics in produced water: A review of process performance, degradation kinetics and pathway. *Chem. Eng. J.* **2022**, *429*, 132492.
  15. Oturan, M.A.; Nidheesh, P. V; Zhou, M. Electrochemical advanced oxidation processes for the abatement of persistent organic pollutants. *Chemosphere* **2018**, *209*, 17–19.
  16. Mirzaei, A.; Chen, Z.; Haghghat, F.; Yerushalmi, L. Removal of pharmaceuticals from water by homo/heterogeneous Fenton-type processes—A review. *Chemosphere* **2017**, *174*, 665–688.
  17. Mejjide, J.; Dunlop, P.S.M.; Pazos, M.; Sanromán, M.A. Heterogeneous electro-Fenton as “Green” technology for pharmaceutical removal: A review. *Catalysts* **2021**, *11*, 85.
  18. Martínez-Huitle, C.A.; Rodrigo, M.A.; Sirés, I.; Scialdone, O. Single and coupled electrochemical processes and reactors for the abatement of organic water pollutants: a critical review. *Chem. Rev.* **2015**, *115*, 13362–13407.
  19. Dewil, R.; Mantzavinos, D.; Poulios, I.; Rodrigo, M.A. New perspectives for advanced oxidation processes. *J. Environ. Manage.* **2017**, *195*, 93–99.
  20. Miron, S.M.; Brendlé, J.; Josien, L.; Fourcade, F.; Rojas, F.; Amrane, A.; Limousy, L. Development of a new cathode for the electro-Fenton process combining carbon felt and iron-containing organic–inorganic hybrids. *Comptes Rendus Chim.* **2019**, *22*, 238–249.
  21. Sruthi, T.; Gandhimathi, R.; Ramesh, S.T.; Nidheesh, P. V. Stabilized landfill leachate treatment using heterogeneous Fenton and electro-Fenton processes. *Chemosphere* **2018**, *210*, 38–43.
  22. Mousset, E.; Wang, Z.; Lefebvre, O. Electro-Fenton for control and removal of micropollutants—process optimization and energy efficiency. *Water Sci. Technol.* **2016**, *74*, 2068–2074.
  23. Brillas, E.; Sirés, I.; Oturan, M.A. Electro-Fenton process and related electrochemical technologies based on Fenton’s reaction chemistry. *Chem. Rev.* **2009**, *109*, 6570–6631.
  24. Moratalla, Á.; Lacasa, E.; Cañizares, P.; Rodrigo, M.A.; Sáez, C. Electro-Fenton-based technologies for selectively degrading antibiotics in aqueous media. *Catalysts* **2022**, *12*, 602.
  25. Sirés, I.; Brillas, E.; Oturan, M.A.; Rodrigo, M.A.; Panizza, M. Electrochemical advanced oxidation processes: today and tomorrow. A review. *Environ. Sci. Pollut. Res.* **2014**, *21*,

8336–8367.

26. Ganzenko, O.; Huguenot, D.; Van Hullebusch, E.D.; Esposito, G.; Oturan, M.A. Electrochemical advanced oxidation and biological processes for wastewater treatment: a review of the combined approaches. *Environ. Sci. Pollut. Res.* **2014**, *21*, 8493–8524.
27. Moreira, F.C.; Boaventura, R.A.R.; Brillas, E.; Vilar, V.J.P. Electrochemical advanced oxidation processes: A review on their application to synthetic and real wastewaters. *Appl. Catal. B Environ.* **2017**, *202*, 217–261.
28. Nidheesh, P.V.; Ganiyu, S.O.; Martínez-Huitle, C.A.; Mousset, E.; Olvera-Vargas, H.; Trelu, C.; Zhou, M.; Oturan, M.A. Recent advances in electro-Fenton process and its emerging applications. *Crit. Rev. Environ. Sci. Technol.* **2022**, 1–27.
29. Ganiyu, S.O.; Martínez-Huitle, C.A.; Oturan, M.A. Electrochemical advanced oxidation processes for wastewater treatment: advances in formation and detection of reactive species and mechanisms. *Curr. Opin. Electrochem.* **2021**, *27*, 100678.
30. Sirés, I.; Brillas, E. Upgrading and expanding the electro-Fenton and related processes. *Curr. Opin. Electrochem.* **2021**, *27*, 100686.
31. Mbaye, M.; Diaw, P.A.; Mbaye, O.M.A.; Oturan, N.; Seye, M.D.G.; Trelu, C.; Coly, A.; Tine, A.; Aaron, J.-J.; Oturan, M.A. Rapid removal of fungicide thiram in aqueous medium by electro-Fenton process with Pt and BDD anodes. *Sep. Purif. Technol.* **2022**, *281*, 119837.
32. Garcia-Rodriguez, O.; Mousset, E.; Olvera-Vargas, H.; Lefebvre, O. Electrochemical treatment of highly concentrated wastewater: A review of experimental and modeling approaches from lab-to full-scale. *Crit. Rev. Environ. Sci. Technol.* **2022**, *52*, 240–309.
33. Ferrag-Siagh, F.; Fourcade, F.; Soutrel, I.; Aït-Amar, H.; Djelal, H.; Amrane, A. Electro-Fenton pretreatment for the improvement of tylosin biodegradability. *Environ. Sci. Pollut. Res.* **2014**, *21*, 8534–8542.
34. Heidari, Z.; Pelalak, R.; Alizadeh, R.; Oturan, N.; Shirazian, S.; Oturan, M.A. Application of mineral iron-based natural catalysts in electro-Fenton process: a comparative study. *Catalysts* **2021**, *11*, 57.
35. Oturan, M.A. Outstanding performances of the BDD film anode in electro-Fenton process: Applications and comparative performance. *Curr. Opin. Solid State Mater. Sci.* **2021**, *25*, 100925.
36. Martínez-Huitle, C.A.; Panizza, M. Electrochemical oxidation of organic pollutants for wastewater treatment. *Curr. Opin. Electrochem.* **2018**, *11*, 62–71.
37. Florenza, X.; Solano, A.M.S.; Centellas, F.; Martínez-Huitle, C.A.; Brillas, E.; Garcia-Segura, S. Degradation of the azo dye Acid Red 1 by anodic oxidation and indirect electrochemical processes based on Fenton's reaction chemistry. Relationship between decolorization, mineralization and products. *Electrochim. Acta* **2014**, *142*, 276–288.

38. Oturan, N.; Bo, J.; Trellu, C.; Oturan, M.A. Comparative performance of ten electrodes in electro-Fenton process for removal of organic pollutants from water. *ChemElectroChem* **2021**, *8*, 3294–3303.
39. dos Santos, A.J.; de Lima, M.D.; da Silva, D.R.; Garcia-Segura, S.; Martínez-Huitle, C.A. Influence of the water hardness on the performance of electro-Fenton approach: Decolorization and mineralization of Eriochrome Black T. *Electrochim. Acta* **2016**, *208*, 156–163.
40. Annabi, C.; Fourcade, F.; Soutrel, I.; Geneste, F.; Floner, D.; Bellakhal, N.; Amrane, A. Degradation of enoxacin antibiotic by the electro-Fenton process: optimization, biodegradability improvement and degradation mechanism. *J. Environ. Manage.* **2016**, *165*, 96–105.
41. Oturan, N.; van Hullebusch, E.D.; Zhang, H.; Mazeas, L.; Budzinski, H.; Le Menach, K.; Oturan, M.A. Occurrence and removal of organic micropollutants in landfill leachates treated by electrochemical advanced oxidation processes. *Environ. Sci. Technol.* **2015**, *49*, 12187–12196.
42. Mousset, E.; Wang, Z.; Hammaker, J.; Lefebvre, O. Physico-chemical properties of pristine graphene and its performance as electrode material for electro-Fenton treatment of wastewater. *Electrochim. Acta* **2016**, *214*, 217–230.
43. Aboudalle, A.; Djelal, H.; Fourcade, F.; Domergue, L.; Assadi, A.A.; Lendormi, T.; Taha, S.; Amrane, A. Metronidazole removal by means of a combined system coupling an electro-Fenton process and a conventional biological treatment: By-products monitoring and performance enhancement. *J. Hazard. Mater.* **2018**, *359*, 85–95.
44. Orimolade, B.O.; Zwane, B.N.; Koiki, B.A.; Rivallin, M.; Bechelany, M.; Mabuba, N.; Lesage, G.; Cretin, M.; Arotiba, O.A. Coupling cathodic electro-Fenton with anodic photo-electrochemical oxidation: A feasibility study on the mineralization of paracetamol. *J. Environ. Chem. Eng.* **2020**, *8*, 104394.
45. Ganiyu, S.O.; de Araújo, M.J.G.; de Araujo Costa, E.C.T.; Santos, J.E.L.; dos Santos, E.V.; Martinez-Huitle, C.A.; Pergher, S.B.C. Design of highly efficient porous carbon foam cathode for electro-Fenton degradation of antimicrobial sulfanilamide. *Appl. Catal. B Environ.* **2021**, *283*, 119652.
46. da Silva Duarte, J.L.; Solano, A.M.S.; Arguelho, M.L.P.M.; Tonholo, J.; Martínez-Huitle, C.A.; e Silva, C.L. de P. Evaluation of treatment of effluents contaminated with rifampicin by Fenton, electrochemical and associated processes. *J. water Process Eng.* **2018**, *22*, 250–257.
47. Adachi, A.; Ouadrhiri, F. El; Kara, M.; El Manssouri, I.; Assouguem, A.; Almutairi, M.H.; Bayram, R.; Mohamed, H.R.H.; Peluso, I.; Eloutassi, N. Decolorization and degradation of methyl orange azo dye in aqueous solution by the electro Fenton process: application

- of optimization. *Catalysts* **2022**, *12*, 665.
48. El Kateb, M.; Trelu, C.; Darwich, A.; Rivallin, M.; Bechelany, M.; Nagarajan, S.; Lacour, S.; Bellakhal, N.; Lesage, G.; Heran, M. Electrochemical advanced oxidation processes using novel electrode materials for mineralization and biodegradability enhancement of nanofiltration concentrate of landfill leachates. *Water Res.* **2019**, *162*, 446–455.
  49. Barhoumi, N.; Olvera-Vargas, H.; Oturan, N.; Huguenot, D.; Gadri, A.; Ammar, S.; Brillas, E.; Oturan, M.A. Kinetics of oxidative degradation/mineralization pathways of the antibiotic tetracycline by the novel heterogeneous electro-Fenton process with solid catalyst chalcopyrite. *Appl. Catal. B Environ.* **2017**, *209*, 637–647.
  50. Nair, K.M.; Kumaravel, V.; Pillai, S.C. Carbonaceous cathode materials for electro-Fenton technology: Mechanism, kinetics, recent advances, opportunities and challenges. *Chemosphere* **2021**, *269*, 129325.
  51. Hammami, S.; Oturan, N.; Bellakhal, N.; Dachraoui, M.; Oturan, M.A. Oxidative degradation of direct orange 61 by electro-Fenton process using a carbon felt electrode: application of the experimental design methodology. *J. Electroanal. Chem.* **2007**, *610*, 75–84.
  52. Vrinceanu, N.; Hlihor, R.M.; Simion, A.I.; Rusu, L.; Fekete-Kertész, I.; Barka, N.; Favier, L. New evidence of the enhanced elimination of a persistent drug used as a lipid absorption inhibitor by advanced oxidation with UV-A and nanosized catalysts. *Catalysts* **2019**, *9*, 761.
  53. Barhoumi, N.; Oturan, N.; Olvera-Vargas, H.; Brillas, E.; Gadri, A.; Ammar, S.; Oturan, M.A. Pyrite as a sustainable catalyst in electro-Fenton process for improving oxidation of sulfamethazine. Kinetics, mechanism and toxicity assessment. *Water Res.* **2016**, *94*, 52–61.
  54. Sopaj, F.; Oturan, N.; Pinson, J.; Podvorica, F.; Oturan, M.A. Effect of the anode materials on the efficiency of the electro-Fenton process for the mineralization of the antibiotic sulfamethazine. *Appl. Catal. B Environ.* **2016**, *199*, 331–341.
  55. Labiadh, L.; Oturan, M.A.; Panizza, M.; Hamadi, N. Ben; Ammar, S. Complete removal of AHPS synthetic dye from water using new electro-Fenton oxidation catalyzed by natural pyrite as heterogeneous catalyst. *J. Hazard. Mater.* **2015**, *297*, 34–41.
  56. Yang, W.; Zhou, M.; Oturan, N.; Bechelany, M.; Cretin, M.; Oturan, M.A. Highly efficient and stable FeII/FeIII LDH carbon felt cathode for removal of pharmaceutical ofloxacin at neutral pH. *J. Hazard. Mater.* **2020**, *393*, 122513.
  57. Sopaj, F.; Oturan, N.; Pinson, J.; Podvorica, F.I.; Oturan, M.A. Effect of cathode material on electro-Fenton process efficiency for electrocatalytic mineralization of the antibiotic sulfamethazine. *Chem. Eng. J.* **2020**, *384*, 331–341.
  58. Oturan, M.A.; Pimentel, M.; Oturan, N.; Sirés, I. Reaction sequence for the

- mineralization of the short-chain carboxylic acids usually formed upon cleavage of aromatics during electrochemical Fenton treatment. *Electrochim. Acta* **2008**, *54*, 173–182.
59. Garcia-Segura, S.; Brillas, E. Mineralization of the recalcitrant oxalic and oxamic acids by electrochemical advanced oxidation processes using a boron-doped diamond anode. *Water Res.* **2011**, *45*, 2975–2984.
  60. Oturan, N.; Ganiyu, S.O.; Raffy, S.; Oturan, M.A. Sub-stoichiometric titanium oxide as a new anode material for electro-Fenton process: Application to electrocatalytic destruction of antibiotic amoxicillin. *Appl. Catal. B Environ.* **2017**, *217*, 214–223.
  61. Yang, W.; Zhou, M.; Oturan, N.; Li, Y.; Oturan, M.A. Electrocatalytic destruction of pharmaceutical imatinib by electro-Fenton process with graphene-based cathode. *Electrochim. Acta* **2019**, *305*, 285–294.
  62. Brillas, E.; Garcia-Segura, S.; Skoumal, M.; Arias, C. Electrochemical incineration of diclofenac in neutral aqueous medium by anodic oxidation using Pt and boron-doped diamond anodes. *Chemosphere* **2010**, *79*, 605–612.
  63. Monteil, H.; Oturan, N.; Péchaud, Y.; Oturan, M.A. Electro-Fenton treatment of the analgesic tramadol: Kinetics, mechanism and energetic evaluation. *Chemosphere* **2020**, *247*.
  64. Yang, W.; Oturan, N.; Raffy, S.; Zhou, M.; Oturan, M.A. Electrocatalytic generation of homogeneous and heterogeneous hydroxyl radicals for cold mineralization of anti-cancer drug imatinib. *Chem. Eng. J.* **2020**, *383*.
  65. Ocampo-Pérez, R.; Sánchez-Polo, M.; Rivera-Utrilla, J.; Leyva-Ramos, R. Degradation of antineoplastic cytarabine in aqueous phase by advanced oxidation processes based on ultraviolet radiation. *Chem. Eng. J.* **2010**, *165*, 581–588.
  66. Ocampo-Pérez, R.; Rivera-Utrilla, J.; Sánchez-Polo, M.; López-Peñalver, J.J.; Leyva-Ramos, R. Degradation of antineoplastic cytarabine in aqueous solution by gamma radiation. *Chem. Eng. J.* **2011**, *174*, 1–8.
  67. Ocampo-Pérez, R.; Sánchez-Polo, M.; Rivera-Utrilla, J.; Leyva-Ramos, R. Enhancement of the catalytic activity of TiO<sub>2</sub> by using activated carbon in the photocatalytic degradation of cytarabine. *Appl. Catal. B Environ.* **2011**, *104*, 177–184.
  68. Ocampo-Pérez, R.; Rivera-Utrilla, J.; Mota, A.J.; Sanchez-Polo, M.; Leyva-Ramos, R. Effect of radical peroxide promoters on the photodegradation of cytarabine antineoplastic in water. *Chem. Eng. J.* **2016**, *284*, 995–1002.